Ferromagnetic ordering and half-metallic state of $Sn_2Co_3S_2$ with the shandite-type structure

W. Schnelle, A. Leithe-Jasper, and H. Rosner
Max-Planck-Institut für Chemische Physik fester Stoffe, Nöthnitzer Straße 40, 01187 Dresden, Germany

F. M. Schappacher and R. Pöttgen
Institut für Anorganische und Analytische Chemie, Universität Münster, Corrensstraße 30, 48149 Münster, Germany

F. Pielnhofer and R. Weihrich
Institut für Anorganische Chemie, Universität Regensburg, Universitätsstraße 31, 93040 Regensburg, Germany
(Received 28 June 2013; published 4 October 2013)

Single crystalline $Sn_2Co_3S_2$ with the shandite-type structure was investigated by magnetization, magnetoresistance, Hall effect, and heat capacity measurements and by ^{119}Sn Mößbauer spectroscopy. $Sn_2Co_3S_2$ orders ferromagnetically at 172 K with an easy-axis magnetization of $\approx 1\ \mu_B$ along the hexagonal c axis. The half-metallic ferromagnetic state is investigated by detailed band-structure calculations by density functional theory (DFT) methods. The magnetoresistance and the Hall effect as well as the DFT results show that ferromagnetic $Sn_2Co_3S_2$ is a compensated metal. The ^{119}Sn Mößbauer spectroscopic data confirm these findings. Large transferred hyperfine fields B_{hf} up to 34.2 T are observed.

DOI: 10.1103/PhysRevB.88.144404 PACS number(s): 71.20.Lp, 75.50.Cc, 75.40.Cx, 76.80.+y

I. INTRODUCTION

Several compounds with the general formula $M_2T_3X_2$ crystallize in the shandite structure isostructural to the mineral $Pb_2Ni_3S_2$.[1] Here M can be Pb, Sn, or In, T the transition metals Ni or Co, and X the chalcogen elements S or Se.[2–6] The compounds in the solid-solution series $Sn_{2-x}In_xCo_3S_2$ have been shown to be all isotypic to shandite. The end-members $x = 0$ and $x = 2$ are metals while ordered $SnInCo_3S_2$ is an insulator[7] which shows for deviations from $x = 1$ interesting n-type as well as p-type semiconducting properties which might be useful for thermoelectric applications.[8,9]

For a different reason, $Sn_2Co_3S_2$ has been investigated in the past decade. This compound orders ferromagnetically (fm) with a Curie temperature T_C of 177 K.[10] For the fm ordered phase a half-metallic state, i.e., the existence of electrons of only one spin polarization at the Fermi level, was proposed theoretically.[10–12] From band-structure calculation they found that the fm transition in this compound is accompanied by the formation of a band gap in the spin-minority direction. Since the Fermi level lies within this gap, $Sn_2Co_3S_2$, which is metallic in the nonmagnetic state, becomes insulating for spin-minority charge carriers.[10] While such materials are highly important for spintronics, only very few ferromagnets with sizable T_C have been proven to be half-metallic. The reliable experimental determination of the conduction electron spin polarization is a challenging task.[13–15] From a classification given in a review by Coey[13] $Sn_2Co_3S_2$ can be assigned to type I_A half-metallic ferromagnets.

Measurements of the magnetic susceptibility[10,16] confirm the results of the bulk band-structure calculation. The fm ordering in $Sn_2Co_3S_2$ rather sensitively depends on the electron count, as demonstrated by substituting Co by Ni[16] or Sn by In.[11,17] For example, with only a few percent of Ni the T_C in $Sn_2(Co_{1-x}Ni_x)_3S_2$ is drastically reduced. For $x > 0.2$ the compound becomes no more fm.[16] This experimental observation is in accordance with band-structure calculations performed for $Sn_2Ni_3S_2$ and the isoelectronic $Pb_2Ni_3S_2$ by Weihrich *et al.*[18] In these compounds with the shandite-type structure, the energy gap in exchange-split transition-metal 3d states is shifted to higher binding energy and ferromagnetism is suppressed. Another important issue reported in Ref. 11 is the influence of Sn and S atoms on electronic properties of $Sn_2Co_{3-x}Ni_xS_2$. Although contributions originating from Sn and S states to the valence-band density of states (DOS) are rather small, particularly S–Sn–S bonds along the [111] direction of the crystals are important for the gap formation. Also by a substitution of S by Se the T_C of $Sn_2Co_3S_{2-x}Se_x$ is affected.[19]

In a previous publication we characterized the electronic structure of the surface of $Sn_2Co_3S_2$ by angle-resolved and core-level photoemission on single crystals and polycrystalline samples.[20] These studies showed that, consistent with theoretical predictions, the region around the Fermi level (E_F) is dominated by Co 3d states. However, due to the fact that the main peak of the photoemission peak is located close to E_F, a clear observation of the energy gap is difficult and angle-resolved data reveal a gap size much smaller than theoretically predicted. Indirect evidence of the half-metallic state comes from the strong shift of the spin majority band below E_F, which is manifested in a significant increase of photoemission intensity. However, no spin-polarized spectroscopic data are currently available for a quantitative determination of the spin polarization at E_F.

To shed more light on the half-metallic fm state and the anisotropic magnetic properties of $Sn_2Co_3S_2$ we extended our study to measurements of the anisotropic magnetization and electrical transport properties as magnetoresistance (MR) and Hall effect, as well as specific heat. In addition, a study of the electronic structure and of the spin polarization in dependence of the structural parameters is presented, pointing out ways to enforce spin polarization in Co-based shandite structures. ^{119}Sn Mößbauer spectroscopic measurements complete the study.

II. EXPERIMENTAL TECHNIQUES

The synthesis of polycrystalline material and the growth of single crystals of $Sn_2Co_3S_2$ by a modified vertical Bridgman technique has been described in detail in Ref. 20. The sample used for the magnetization and heat capacity study was mechanically extracted from a crystal[20] and metallographically characterized. By wavelength- and energy-dispersive x-ray spectroscopy a chemical composition of $Sn_{2.0(1)}Co_{3.0(1)}S_{1.9(1)}$ was deduced. Lattice parameters were least-squares refined on Guinier powder x-ray diffraction data [Huber image plate camera G670, CoK_α radiation with $\lambda = 1.78897$ Å; NIST standard LaB_6 with $a = 4.15692(1)$ Å] and are in good agreement with previous single crystal data.[4,11]

The magnetization was measured in a commercial magnetometer (MPMS XL-7, Quantum Design) equipped with a 360° horizontal rotator. For this measurement a part of the crystal was cut to an oriented cube and glued to the rotator axis with GE 7031 varnish.

Heat capacity was measured on the same sample and on a polycrystalline sample of $In_2Co_3S_2$ with a relaxation-type method (PPMS, Quantum Design).

Electrical transport properties (transverse and longitudinal magnetoresistivity, Hall effect) were measured on a bar-shaped crystal with current flow along the crystallographic c direction (hexagonal setting). The measurements were made with a low-frequency alternating current.

A $Ca^{119m}SnO_3$ source was available for the ^{119}Sn Mößbauer spectroscopic investigations. The $Sn_2Co_3S_2$ powder sample was placed within a thin-walled glass container at a thickness of about 10 mg Sn cm^{-2}. A palladium foil of 0.05 mm thickness was used to reduce the tin K-line x rays concurrently emitted by this source. The measurements were conducted in the usual transmission geometry between 77 K and room temperature.

For the electronic structure calculations the full-potential local-orbital scheme FPLO[21] (versions: fplo5.00-19, fplo9.01-35) within the local (spin) density approximation (LDA/LSDA) and the generalized gradient approximation (GGA) were used. In the scalar relativistic and fully relativistic calculations the exchange and correlation potential of Perdew and Wang[22] (LDA) and Perdew, Burke, and Ernzerhof[23] (GGA) were chosen. Well converged k meshes of at least $12 \times 12 \times 12$ have been used throughout the calculations.

III. RESULTS AND DISCUSSION

A. Crystal structure

Based on powder neutron and single-crystal x-ray diffraction data the crystal structure of $Sn_2Co_3S_2$ has been refined and discussed in previous publications.[7,10,11,24] Lattice parameters of the rhombohedral crystal structure (hexagonal setting, space group $R\bar{3}m$) of the sample used in this study [$a = 5.3672(3)$ Å, $c = 13.1765(7)$ Å, $T = 293$ K] are in good agreement with those previous data.

The crystal structure of $Sn_2Co_3S_2$ is depicted in Fig. 1. The coordination polyhedron of Co, which is composed of 2 Sn1 and 2 Sn2 atoms as well as 2 S atoms being in close contact [d(Co–S) = 2.18 Å, d(Co–Sn) = 2.68 Å], is a tetragonal bipyramid. The staggered A–B–C stacking along the c axis (hexagonal setting) of the face-sharing bipyramids is

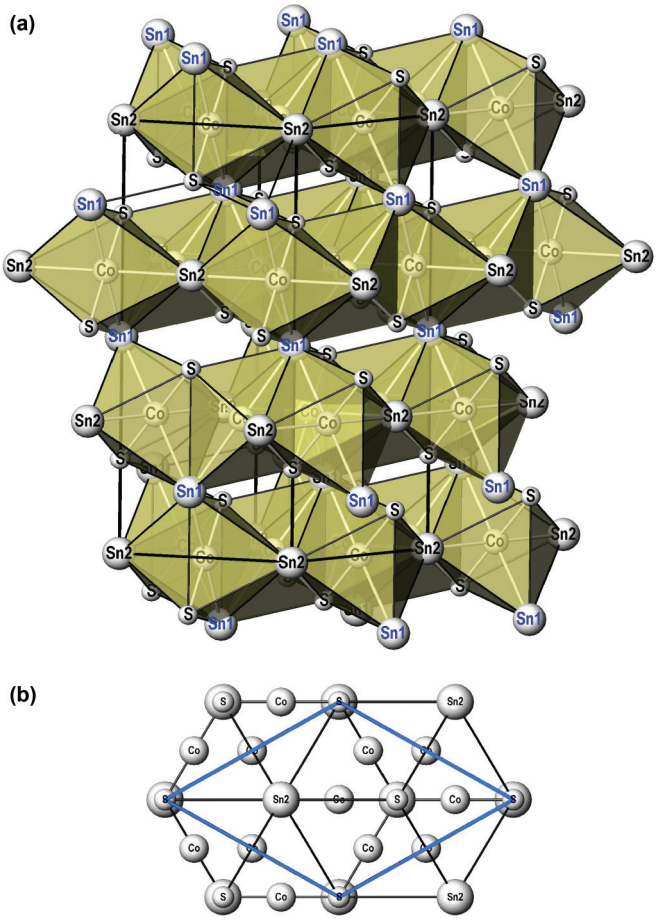

FIG. 1. (Color online) (a) Shandite-type crystal structure of $Sn_2Co_3S_2$ in the hexagonal setting. (b) Projection along [001]. The unit cell of the rhombohedral setting is outlined (blue).

outlined in Fig. 1(a). Co atoms occupy the 9e ($\frac{1}{2}$,0,0) position in the basal plane in a Kagome-net-like arrangement [Fig. 1(b)]. There are two independent Sn positions [Sn(1) on 3b (0,0,$\frac{1}{2}$), Sn(2) on 3a (0,0,0)]. While Sn1 atoms are situated above and below and thus interconnect the slabs, Sn2 is incorporated within the layers and therefore shows a hexagonal-planar coordination by Co atoms with additional contacts to sulfur. Sulfur is located on a 6c (0,0,0.2172) position.[7]

B. Magnetic properties

The magnetic susceptibility M/H in the paramagnetic regime shows a field dependence which is—for the most part—due to minor impurities of Co metal or similar fm impurities with $T_C > 400$ K. Considering only the two highest external field curves [Fig. 2(a), inset] it is remarkable that for $T > 250$ K the susceptibility M/H for $H_{ext} = 35$ kOe is slightly larger than for $H_{ext} = 70$ kOe, in contrast to the expectation for a paramagnet with small fm impurities. We attribute this effect to the dampening of spin fluctuations by an external field.

The effective moment μ_{eff} and the Weiss parameter θ_W derived from fitting a Curie-Weiss law to M/H_{ext} above 240 K for $H_{ext} = 70$ kOe are 1.72 μ_B/f.u. and +183 K, respectively. As for the fm half-metallic skutterudites {Na/K/Tl}Fe_4Sb_{12},[25,26]

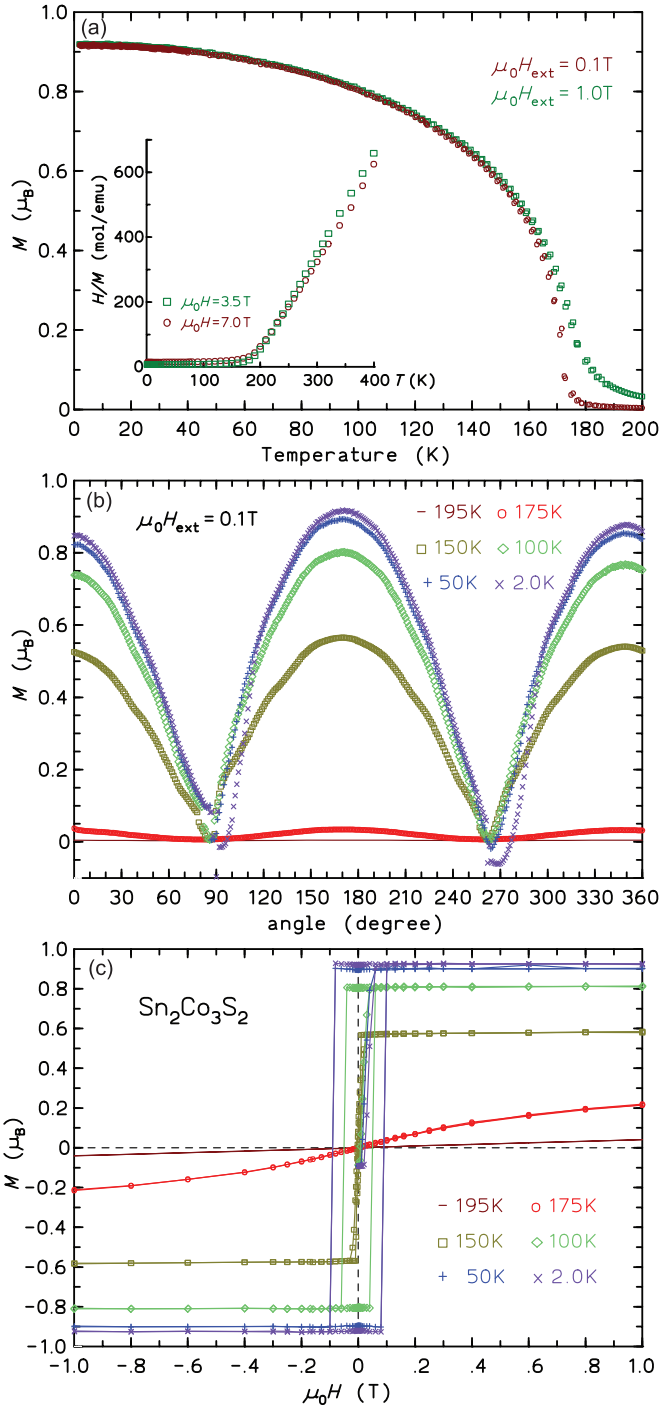

FIG. 2. (Color online) (a) Longitudinal magnetization $M(T)$ (magnetic moment detection parallel to the applied field) of the $Sn_2Co_3S_2$ single crystal for magnetic fields along the easy axis. The inset shows the inverse susceptibility H/M of polycrystalline material up to $T = 400$ K for high fields. (b) Longitudinal magnetization of the crystal for different angles of the magnetic field with the hexagonal c axis. The easy axis ($H \| c$) lies at 172° in this experimental setup. (c) Isothermal magnetization loops of the crystal for field along the easy axis.

the μ_{eff} corresponds to the pseudospin 1/2 of one electron. The T_C, μ_{eff}, and θ_W values are in agreement with previous measurements on polycrystalline material[11] and single crystals.[27]

In the fm state the field cooled magnetization of the single crystal with the applied field along the easy axis (which is the hexagonal c axis, see below) varies in the usual manner with temperature below $T_C = 172$ K [Fig. 2(a)]. This Curie temperature is ≈5 K lower than previously reported for polycrystalline material.[10] At $T = 1.8$ K a moment of 0.92 μ_B/f.u. is attained at $H_{\text{app}} = 1.0$ T for the single crystal.

In Fig. 2(b) the dependence of the longitudinal magnetization (the component parallel to the applied field) for a rotation of the crystal around an axis lying in the hexagonal a plane is shown. Mainly due to the shape and size of the sample and its asymmetric mounting position on the flattened top of the rotator axis, the maximum of the magnetization is found at 172°, the other maxima at nominally zero and 360° being lower. The data shown in Figs. 2(a) and 2(c) were recorded for this experimentally obtained angle setting, i.e., for the easy axis of the sample piece which coincides—within experimental error—with the hexagonal c axis.

The magnetization loops (for the rotator angle 172°) for selected temperatures are given in Fig. 2(c). The loops are square for all temperatures well below T_C, as expected for easy-axis $M(H)$ curves within the Stoner-Wohlfarth model. For $T = 2$ K the initial curve increases only little up to fields of 0.02 T, where M starts to rise linearly. The coercive field $\mu_0 H_c$ for this temperature is only 0.08–0.10 T. It decreases to ≈0.05 T for $T = 100$ K. At $T = 2$ K the saturation moment is 0.93 μ_B/f.u. at 1.0 T and the remanence is only slightly smaller.

C. Specific heat

At the Curie point a pronounced λ-type anomaly is observed in the specific heat capacity (Fig. 3). The size of the anomaly together with the magnetization demonstrates the formation of the bulk fm ground state of $Sn_2Co_3S_2$. In order to estimate the entropy involved in the magnetic anomaly, the specific heat of the isostructural compound $In_2Co_3S_2$, which does not order magnetically, was measured. The magnetic entropy S_{mag}, which varies for itinerant magnets in wide ranges, may

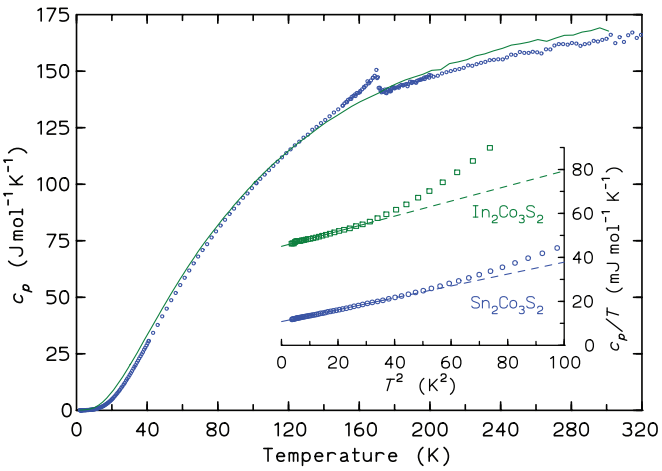

FIG. 3. (Color online) Molar heat capacity $c_p(T)$ of single crystalline $Sn_2Co_3S_2$ (circles) and of polycrystalline $In_2Co_3S_2$ (line) in zero field. The inset shows c_p/T vs T^2 at low T and the fits to $c_p(T) = \gamma T + \beta T^3$ (see text).

give a measure for the modifications at the Fermi surface at T_C. Unfortunately, the phonon contribution of the In compound seems to be quite different from that of the Sn compound and no quantitative estimate of S_{mag} is possible. The transition does not show a temperature hysteresis and no indications are found for a latent heat. Together with the x-ray diffraction results,[11,18,24] which show no obvious lattice effects, we conclude that the transition is of second order and no significant magnetostructural coupling is present.

At low temperatures $c_p(T)$ (see inset of Fig. 3) approximates the Debye T^3 behavior plus a linear (electronic) term $c_p(T) = \gamma T + \beta T^3$. From a fit up to 6 K we obtain $\gamma = 10.8$ mJ mol^{-1} K^{-2} and β corresponding to an initial Debye temperature $\Theta_D = 369$ K. For $In_2Co_3S_2$ we observe stronger deviations from the Debye T^3 law, which seem not to be due to spin fluctuations since the specific heat is not changed by magnetic fields up to 9 T. A fit in the temperature range up to 5.5 K leads to $\gamma = 45.0$ mJ mol^{-1} K^{-2} and β corresponding to an initial Debye temperature $\Theta_D = 341$ K. The larger Sommerfeld coefficient indicates that the electronic DOS of this nonmagnetic compound is about four times higher than for fm $Sn_2Co_3S_2$. The exchange split of the electronic states at E_F in fm ordered $Sn_2Co_3S_2$ obviously leads to a smaller DOS as in its nonmagnetic counterpart.

D. Transport properties

The electrical resistivity ρ_{xx} of the $Sn_2Co_3S_2$ crystal measured in c direction [Fig. 4(a)] at 1.8 K is high ($\approx$0.70 $\mu\Omega$ m) and increases only to $\approx$1.84 $\mu\Omega$ m at 300 K. The overall temperature dependence is that of a metal. The small residual resistance ratio indicates a nonoptimal quality of the bar cut from the crystal. At T_C a change of slope $d\rho/dT$ is observed, which is consistent with the few data points given in Ref. 5.

In the inset of Fig. 4(a) the Hall constant R_H as a function of temperature is given. The Hall constant was determined from the linear portions of ρ_{xy} as a function of the applied field. Well below T_C linear portions were typically observed ± 3 T only, for $T > 200$ K in the full field range ± 9 T. For the isotherms between 40 and 140 K an small anomalous Hall effect has been observed in the field range of the magnetic hysteresis which has been considered in the calculation of the normal R_H. For temperatures around T_C the Hall effect cannot be determined reliably. The Hall constant R_H of polycrystalline $In_2Co_3S_2$ shows only a weak increase with increasing temperature (7–10$\times 10^{-10}$ m^3/C) without any anomaly.

For the lowest temperatures R_H is negative, indicating that the majority of carriers at E_F are electrons. R_H increase with T and becomes positive at $\approx$35 K, signaling that carriers from more than one band are present in the fm state. This is consistent with the results from our electronic structure calculation (see below, Fig. 7). At room temperature we have again a negative but comparatively small Hall constant. It has to be mentioned that the Hall constants measured in a polycrystalline piece showed the same crossovers between negative and positive R_H regimes but with strongly differing scale. This can be expected since with the crystal we probed only R_H for current parallel to the hexagonal c direction. The size of the anomalous Hall effect increases from

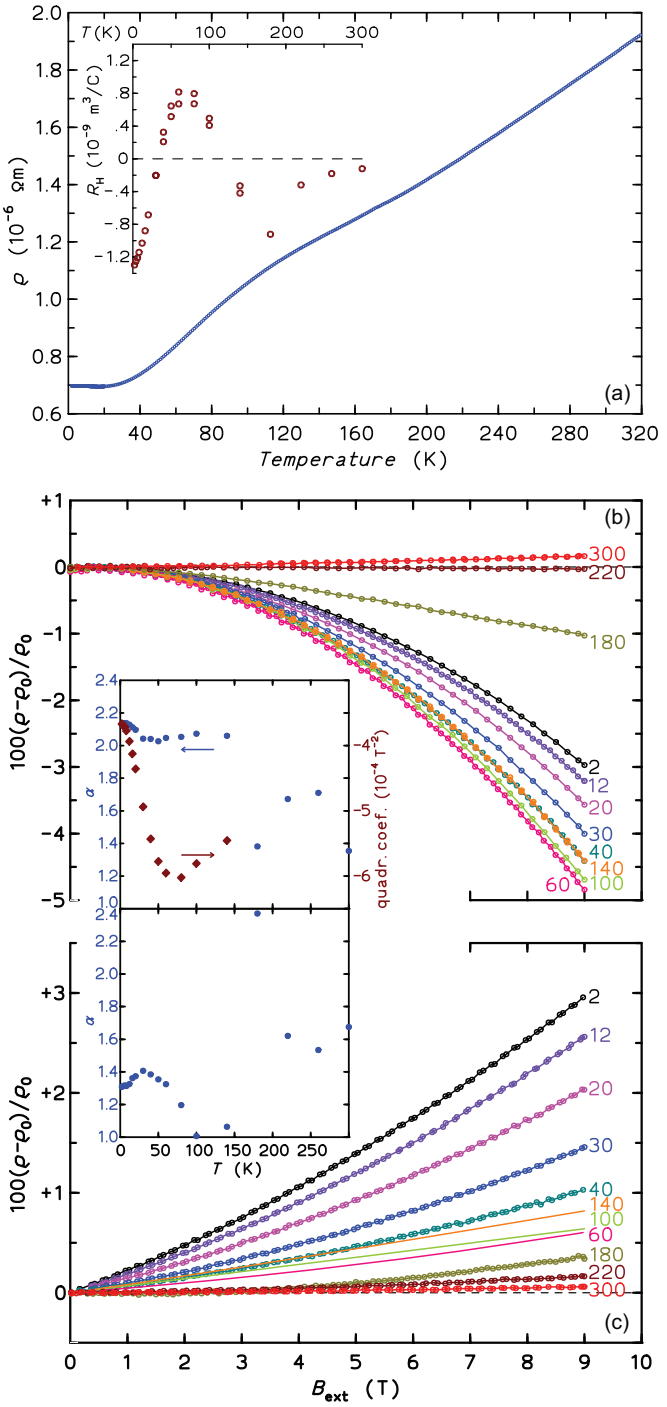

FIG. 4. (Color online) (a) Electrical resistivity $\rho(T)$ along the hexagonal c direction of single-crystalline $Sn_2Co_3S_2$. The inset shows the temperature dependence of the Hall constant $R_H = \rho_{xy}/H$. (b) Relative transversal (TMR, $H \perp c \| j$) and (c) longitudinal (LMR, $H \| c \| j$) magnetoresistance $MR = \rho(H)/\rho_0 - 1$ vs external magnetic field $\mu_0 H$ for selected temperatures. The insets show the results of power law fits to the TMR and LMR data, respectively. In TMR exponents α close to 2.0 are observed in the fm state. The inset for the TMR also shows the coefficient A for this observed quadratic field dependence

-0.46×10^{-9} Ω m at 80 K to -2.27×10^{-9} Ω m at 140 K. It is not proportional to the saturation magnetization.

In Figs. 4(b) and 4(c) the transversal (TMR, $H \perp c \| j$) and longitudinal (LMR, $H \| c \| j$) magnetoresistance $\rho(H)/\rho_0 - 1$ as a function of the external magnetic field are presented [$\rho_0 = \rho(H = 0)$]. Generally, TMR is negative in the fm regime while LMR is positive. Obviously both TMR and LMR do not obey Kohler's rule. Both may be described by general power laws MR $= AB_{\text{ext}}^{\alpha}$. The results of such fits are summarized in the insets of Figs. 4(b) and 4(c), respectively. For the TMR, exponents close to 2.0 are observed within the fm regime. Such a quadratic field dependence is the hallmark of a compensated metal[28] with an equal amount of electrons and holes at the Fermi surface.[28,29] In Sec. III F we will show that this is actually the case for $Sn_2Co_3S_2$. Fitting the quadratic field dependence TMR $= AT^2$, we find the temperature dependence of the coefficient A [inset Fig. 4(b)]. The quadratic dependence is strongest for $T \approx 70$ K. Above T_C (e.g., at $T = 180$ K), the TMR is still negative due to the presence of fm fluctuations, while it is much smaller and positive at 300 K.

The positive LMR follows for $T \leqslant 80$ K a power law with an exponent $\approx$1.3 [Fig. 4(c) inset]. The size of the LMR (coefficient of the power law) decreases with temperature up to $\approx$70 K and then increases again slightly. In the paramagnetic range a small positive LMR is observed (the power law cannot be determined here). All MR isotherms do not show saturating behavior, i.e., the exponents α are larger than 1.0 in the covered field range.

E. ^{119}Sn Mößbauer spectroscopy

The ^{119}Sn spectra of $Sn_2Co_3S_2$ are presented in Fig. 5 together with transmission integral fits. The corresponding fitting parameters are listed in Table I. For the investigated temperature range the spectra are composed of two subsets of almost equal contribution, in agreement with the two crystallographically independent tin sites (both with site symmetry $\bar{3}m$).[11,18] At 298 K we observe a superposition of two quadrupole split signals at almost similar isomer shifts. The strong quadrupole splitting results from the noncubic site symmetry of the tin atoms. We observe only little variation of the isomer shift with temperature. The isomer shift of $Sn_2Co_3S_2$ (2.14 mm s^{-1} at 298 K) is smaller than for isotypic $Sn_2Ni_3S_2$ (2.48 mm s^{-1} at 300 K),[30] indicating lower electron density at the tin nuclei in the cobalt compound. Similar to $Sn_2Ni_3S_2$ the isomer shift is indicative for divalent tin, however, in comparison to SnS ($\delta = 3.4$ mm s^{-1}) and other binary divalent tin compounds[31] the isomer shift is rather low and is closer to values typically observed for intermetallic tin compounds like $CaPdSn_2$,[32] or the series $PdSn_x$ ($x = 2, 3, 4$).[33] Similar conclusions are based on core-level photoemission data which do not support a valence state +2 of Sn. Therefore, no shift of the Sn $4d_{5/2}$ peak to higher binding energies indicative of a Sn^{2+} configuration was observed.[20]

At 140 K, slightly below $T_C = 172$ K, we observe significant hyperfine (hf) field splitting of both tin sites (*transferred* hf fields originating from the electron spin polarization by the strongly polarized Co atoms). One of the tin sites, however, shows a substantially higher hf field, 22.3 T vs 9.4 T at 140 K. These hf fields increase to the huge value of 34.2 T for the first and to 11.2 T for the second signal. The magnetic

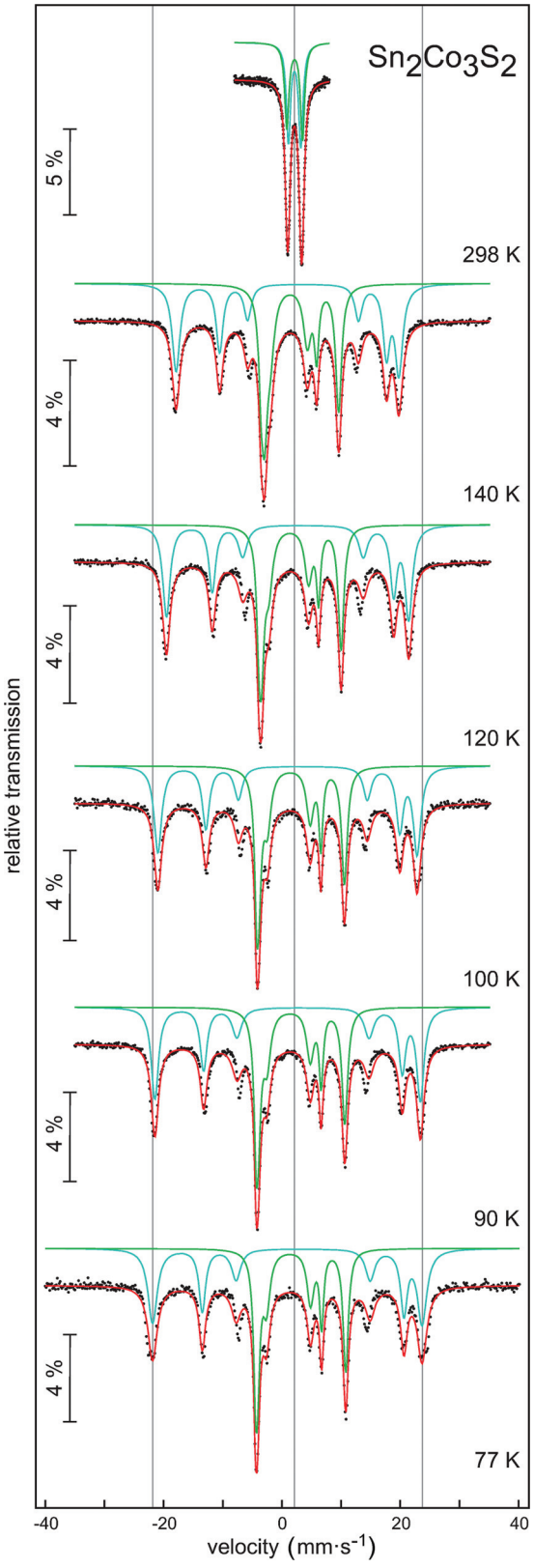

FIG. 5. (Color online) Experimental and simulated ^{119}Sn Mößbauer spectra of $Sn_2Co_3S_2$ at different temperatures.

hf field splitting is associated with a reduction in the electric field gradient (EFG) of the first tin site used to optimize the least-squares fits to the data (Table I), indicating a change

TABLE I. Fitting parameters of ^{119}Sn Mößbauer spectroscopic measurements of $Sn_2Co_3S_2$: (δ) isomer shift; (ΔE_Q) electric quadrupole splitting; ($|B_{hf}|$) magnetic hyperfine field; (Γ) experimental linewidth; and (A_1:A_2) area ratio.

T (K)	δ_1 (mm s^{-1})	ΔE_{Q1} (mm s^{-1})	B_{hf1} (T)	Γ_1 (mm s^{-1})	δ_2 (mm s^{-1})	ΔE_{Q2} (mm s^{-1})	B_{hf2} (T)	Γ_2 (mm s^{-1})	A_1:A_2
298	2.14(1)	+2.09(1)	–	0.84(1)	2.15(1)	2.65(1)	–	0.88(1)	53:47
140	2.25(1)	−2.63(1)	28.33(1)	1.49(3)	2.25(1)	2.16(1)	9.42(1)	1.60(2)	48:52
120	2.26(1)	−2.60(1)	30.30(1)	1.82(5)	2.21(1)	2.13(1)	10.11(1)	1.56(3)	50:50
100	2.24(1)	−2.59(1)	32.93(1)	1.64(6)	2.23(1)	2.16(1)	10.91(1)	1.48(4)	50:50
90	2.26(1)	−2.59(1)	33.74(1)	1.92(5)	2.21(1)	2.16(1)	11.04(1)	1.50(2)	50:50
77	2.25(1)	−2.67(1)	34.23(1)	1.94(8)	2.21(1)	2.21(1)	11.23(1)	1.36(2)	51:49

in the orientation of the EFG principal axis with respect to the magnetic hf field direction. According to the respective assignment of V_{zz} components of the EFG we attribute the large hf field to Sn(2) within the layers and the smaller one to the Sn(1) position between them. A recent publication gives full account on the EFG calculation.[7] Similar behavior has been observed for EuPdIn[34] and $Eu_2Si_5N_8$[35] in the magnetically ordered state.

F. DFT calculations

A description of the band structure based on spin-polarized and unpolarized calculations as well as the formation of a half-metallic state has been given in detail in previous publications.[11,20] These theoretical studies motivated a detailed photoemission analysis of the surface states and their dispersion relations. The good compatibility of observed and calculated valence-band and angle-resolved photoemission spectra demonstrated that all valence states are rather extended thus justifying a theoretical approach based on LSDA.[12,20]

To get deeper insight into the fm, half-metallic electronic structure of $Sn_2Co_3S_2$ we investigated the stability with respect to the influence of (i) structural parameters, (ii) spin-orbit coupling, and (iii) the choice of the applied exchange-correlation potential (LDA vs GGA). We find that the half-metallic properties are rather robust with respect to the latter issue, only the calculated anisotropy is significantly larger within the GGA (see Supplemental Material,[36] Fig. S1). The main result is the fragility of the half-metallic state with respect to small structural changes (see Fig. 6). Upon reduction of the rhombohedral lattice parameter a by about 1% from the equilibrium value (by about 3% from the experimental value), the half-metallic gap closes completely. This can be understood due to the decrease of the in-plane Co-Co distance, resulting in an increase of the related bandwidth and accordingly the decrease of the half-metallic gap. Further reduction of a yields a fast decrease of the total spin polarization, pointing towards a strong pressure dependence of the magnetic state of $Sn_2Co_3S_2$. A related slight decrease of the Co-S distance (corresponding to an increase of the position parameter x, see Fig. 6) would act in the same way, though less drastic.

The explicit inclusion of spin-orbit coupling, mixing the two spin channels, has only a minor influence on the magnetic moment, reducing it by less than 0.1%, only. From the fully relativistic calculations, we estimated the magnetic anisotropy. In agreement with the experimental observations, we obtain an [001] easy axis anisotropy of about 5 K within LDA (9 K within GGA) with respect to the basal plane which shows almost isotropic behavior (comparing the [100] and [110] directions).

The exchange split of the DOS in the fm state reduces the DOS value at E_F drastically by about a factor of 5 (see Supplemental Material,[36] Fig. S2). The electronic states at E_F in the fm state have predominantly $3d_{z^2-r^2}$ character. We find a bare Sommerfeld coefficient $\gamma_b = 4$ mJ mol^{-1} K^{-2}. This is significantly smaller than the measured $\gamma = 10.8$ mJ mol^{-1} K^{-2}, which hints for a strong renormalization due to many body effects. The contributions of the individual bands to the spin-polarized DOS is presented in Fig. 7. The spin

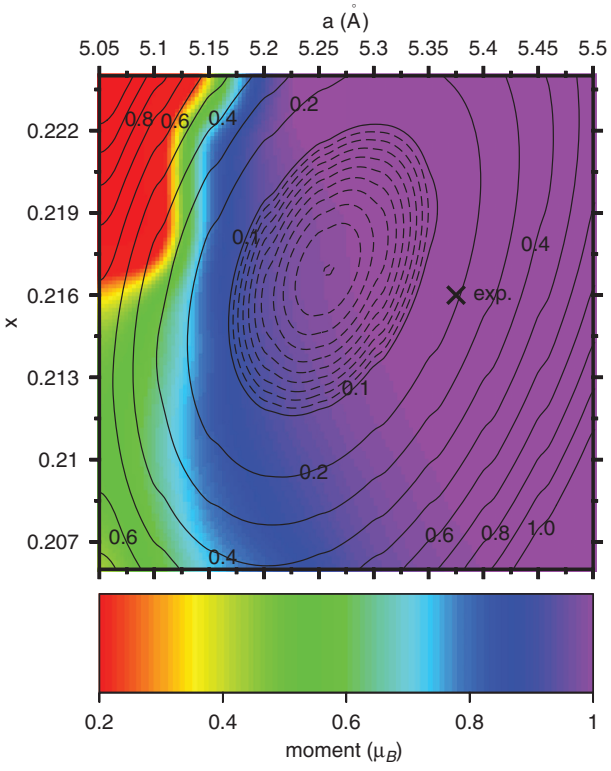

FIG. 6. (Color online) Calculated map of the magnetic polarization (in μ_B per f.u.) in dependence of the rhombohedral lattice parameter a and the sulfur Wyckoff position (x,x,x). The lines are isolines for the calculated total energy (in eV). The energy of the fully optimized structure is set to zero, the energy difference between two adjacent isolines is 0.01 eV/f.u. for the inner (dashed) lines and 0.1 eV/f.u. for the outer (solid) lines. The experimental structure parameters are marked by a cross.

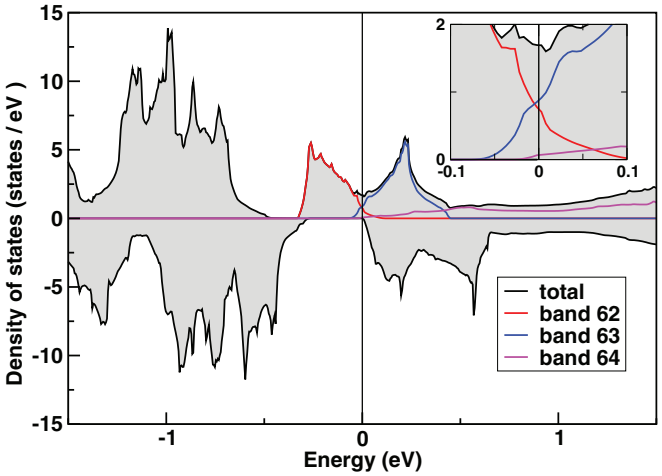

FIG. 7. (Color online) Spin-polarized DOS per formula unit of $Sn_2Co_3S_2$. The contributions of the individual bands is shown. The inset is a magnification around E_F.

polarization of the electrons at E_F is clearly visible. Moreover, the peaks on both sides of E_F originate almost exclusively from two bands (Nos. 62 and 63) with dominant Co 3*d* character. At E_F the electron-type band 63 has a slightly larger partial DOS than the hole-type band 62. Band 64 gives only a minor contribution and is of electron type.

The three bands (Fig. 7) have been analyzed for their Fermi velocities (for pictures of the Fermi surfaces see the Supplemental Material,[36] Fig. S3). All Fermi surface sheets indicate the three-dimensional electronic structure of the compound. The dominating contributions to the DOS at E_F originate from the hole surface of band 62 and the electron surface of band 63. The Fermi velocities of these two surfaces are rather similar, thus resulting in an almost complete compensation of the related charge carriers. The small electron surface from band 64 has a minor influence on the electronic properties since it contributes only a small DOS (see Fig. 7) and also shows small Fermi velocities. These findings explain the negative sign of the Hall effect at $T = 2$ K and the crossover to positive R_H in the fm regime. Thus, $Sn_2Co_3S_2$ in the fm state is a prototypical compensated metal,[28,29] showing a low Hall coefficient and a typical quadratic transverse magnetoresistance (Sec. III D).

IV. SUMMARY

A large single crystal of a rhombohedral shandite-type $Sn_2Co_3S_2$ has been grown and investigated thoroughly. As previously reported for polycrystalline material, the compound orders ferromagnetically at $T_C = 172$ K. The easy axis of the magnetic moment is found to be along the crystallographic *c* direction (hexagonal setting of the rhombohedral structure). The ordered moment of 0.93 μ_B/f.u. is very close to the calculated one (1 μ_B/f.u.), signaling a half-metallic ferromagnetic ground state. As shown by Hall effect and magnetoresistance measurements as well as DFT calculations, the ferromagnet is a compensated metal with a small remaining density of states compared to the isostructural paramagnetic compound $In_2Co_3S_2$. The ^{119}Sn Mößbauer spectroscopy results are in line with these findings. The half-metallic state and the concomitant spin polarization are quite fragile in $Sn_2Co_3S_2$, as demonstrated by a systematic exploration of the structural parameter space.

ACKNOWLEDGMENTS

We are indebted to M. Holder for cutting the crystal and to R. Koban for assistance with the measurements. R.W. gratefully acknowledges the Deutsche Forschungsgemeinschaft (DFG) for financial support (WE42847-1).

[1] P. Ramdohr, Sitz. Berl. Akad. Wiss. Math.-Nat. Kl. **VI**, 1 (1949).
[2] M. Zabel, S. Wandinger, and K. Range, Rev. Chim. Miner. **20**, 698 (1983).
[3] A. Michelet, G. Collin, and O. Gorochov, J. Less-Common Met. **97**, 73 (1984).
[4] M. Zabel, S. Wandinger, and K. Range, Z. Naturforsch. **34B**, 238 (1979).
[5] S. Natarajan, G. V. Subba Rao, R. Baskaran, and T. S. Radhakrishnan, J. Less-Common Met. **138**, 215 (1988).
[6] R. Weihrich, S. F. Matar, V. Eyert, F. Rau, M. Zabel, M. Andratschke, I. Anusca, and T. Bernert, Prog. Solid State Chem. **35**, 309 (2007).
[7] J. Rothballer, F. Bachhuber, F. Pielnhofer, F. M. Schappacher, R. Pöttgen, and R. Weihrich, Eur. J. Inorg. Chem. **2013**, 248 (2013).
[8] J. Corps, P. Vaqueiro, and A. V. Powell, J. Mater. Chem. A **1**, 6553 (2013).
[9] M. Fujioka, T. Sibuya, J. Nakai, K. Yoshiyasu, Y. Takano, Y. Kamihara, and M. Matoba, arXiv:1211.4467.
[10] R. Weihrich, A. C. Stückl, M. Zabel, and W. Schnelle, Z. Anorg. Allg. Chem. **630**, 1767 (2004).
[11] R. Weihrich and I. Anusca, Z. Anorg. Allg. Chem. **632**, 1531 (2006).
[12] Y. S. Dedkov, M. Holder, S. L. Molodtsov, and H. Rosner, J. Phys.: Conf. Series **100**, 072011 (2008).
[13] J. M. D. Coey and S. Sanvito, J. Phys. D: Appl. Phys. **37**, 988 (2004).
[14] C. Utfeld, S. R. Giblin, J. W. Taylor, J. A. Duffy, C. Shenton-Taylor, J. Laverock, S. B. Dugdale, M. Manno, C. Leighton, M. Itou, and Y. Sakurai, Phys. Rev. Lett. **103**, 226403 (2009).
[15] Goutam Sheet, H. Rosner, S. Wirth, A. Leithe-Jasper, W. Schnelle, U. Burkhardt, J. A. Mydosh, P. Raychaudhuri, and Yu. Grin, Phys. Rev. B **72**, 180407(R) (2005).
[16] T. Kubodera, H. Okabe, Y. Kamihara, and M. Matoba, Physica B **378–380**, 1142 (2006).
[17] A. Umetani, E. Nagoshi, T. Kubodera, and M. Matoba, Physica B **493**, 1356 (2008).
[18] R. Weihrich, I. Anusca, and M. Zabel, Z. Anorg. Allg. Chem. **631**, 1463 (2005).
[19] Y. Sakai, Y. Kamihara, and M. Matoba, Phys. Status Solidi C **10**, 1130 (2013).

[20]M. Holder, Y. S. Dedkov, A. Kade, H. Rosner, W. Schnelle, A. Leithe-Jasper, R. Weihrich, and S. L. Molodtsov, Phys. Rev. B **79**, 205116 (2009).
[21]K. Koepernik and H. Eschrig, Phys. Rev. B **59**, 1743 (1999).
[22]J. P. Perdew and Y. Wang, Phys. Rev. B **45**, 13244 (1992).
[23]J. P. Perdew, K. Burke, and M. Ernzerhof, Phys. Rev. Lett. **77**, 3865 (1996).
[24]P. Vaqueiro and G. C. Sobany, Solid State Sci. **11**, 513 (2009).
[25]W. Schnelle, A. Leithe-Jasper, H. Rosner, R. Cardoso-Gil, R. Gumeniuk, D. Trots, J. A. Mydosh, and Yu. Grin, Phys. Rev. B **77**, 094421 (2008).
[26]A. Leithe-Jasper, W. Schnelle, H. Rosner, R. Cardoso-Gil, M. Baenitz, J. A. Mydosh, Yu. Grin, M. Reissner, and W. Steiner, Phys. Rev. B **77**, 064412 (2008).
[27]X. Lin, S. L. Budko, and P. C. Canfield, Philos. Mag. (London) **92**, 2436 (2012).
[28]E. Fawcett and W. A. Reed, Phys. Rev. **131**, 2463 (1963).
[29]A. B. Pippard, *Magnetoresistance in Metals* (Cambridge University Press, Cambridge, 1989).
[30]P. Gütlich, K. Range, C. Felser, C. Schultz-Münzenberg, W. Tremel, D. Walcher, and M. Waldeck, Angew. Chemie Int. Ed. Engl. **38**, 2381 (1999).
[31]P. E. Lippens, Phys. Rev. B **60**, 4576 (1999).
[32]R.-D. Hoffmann, D. Kußmann, U. C. Rodewald, R. Pöttgen, C. Rosenhahn, and B. D. Mosel, Z. Naturforsch. **54B**, 709 (1999).
[33]J. Nylén, F. J. García García, B. D. Mosel, R. Pöttgen, and U. Häussermann, Solid State Sci. **6**, 147 (2004).
[34]H. A. Höppe, H. Trill, B. D. Mosel, H. Eckert, G. Kotzyba, R. Pöttgen, and W. Schnick, J. Phys. Chem. Solids **63**, 853 (2002).
[35]M. Tampier, D. Johrendt, R. Pöttgen, G. Kotzyba, C. Rosenhahn, and B. D. Mosel, Z. Naturforsch. **57B**, 133 (2002).
[36]See Supplemental Material at http://link.aps.org/supplemental/10.1103/PhysRevB.88.144404 for the Figs. S1–S3 presenting further results of the electronic structure calculations for $Sn_2Co_3S_2$ and $In_2Co_3S_2$.